

Predicting nitrogen dioxide column density from the International Wealth Index with a convolutional neural network in Africa

Downloaded from: https://research.chalmers.se, 2026-11-22 01:21 UTC

Citation for the original published paper (version of record):

Grieco, F., Kakooei, M., Daoud, A. (2026). Predicting nitrogen dioxide column density from the International Wealth Index with a
convolutional neural network in Africa. Scientific Reports, 16(1).
http://dx.doi.org/10.1038/s41598-026-73707-0

N.B. When citing this work, cite the original published paper.

research.chalmers.se offers the possibility of retrieving research publications produced at Chalmers University of Technology. It covers all kind of research output: articles, dissertations, conference papers, reports etc. since 2004. research.chalmers.se is administrated and maintained by Chalmers Library

(article starts on next page)

scientific reports

Check for updates

OPEN

Predicting nitrogen dioxide column density from the International Wealth Index with a convolutional neural network in Africa

Francesco Grieco[1,2]✉, Mohammad Kakooei[2,3] & Adel Daoud[1,2]

In the pursuit of improving socioeconomic living conditions of their populations, many nations struggle to meet their nationally determined contributions (NDCs) under the Paris agreement, and that shortfall makes accountability for emissions reductions critical. The long atmospheric lifetimes of key gases such as carbon dioxide (CO_2) and methane (CH_4) hinder traditional greenhouse gas (GHG) monitoring, because what any one place emits adds only a small excess to a large, well-mixed background. Nitrogen dioxide (NO_2) behaves differently: it is short-lived and highly variable in space and time, so satellite instruments resolve its patterns close to source regions. Across the African continent, mapped temporal correlations between NO_2 and CO_2 are moderate in magnitude but spatially structured and consistently positive. Although we do not use that association to mechanically convert NO_2 observations into CO_2, we report it as contextual evidence towards NDCs. Given this context, this study asks the following question: to what extent can socioeconomic development at the neighbourhood scale predict NO_2 column densities (the amount of NO_2 in the air column above that neighbourhood) across Africa? We apply a convolutional neural network (CNN) to gridded International Wealth Index (IWI) estimates and to NO_2 observations from the tropospheric Monitoring Instrument (TROPOMI), and obtain an average predictive accuracy of $R^2 = 0.56$ across the African continent. Because IWI can be projected forward, we also present an illustrative 2030 scenario as a methodological demonstration of the relationship between socioeconomic development and NO_2 trajectories. These findings indicate that gridded wealth estimates carry predictive information about NO_2 column density in Africa. Such estimates offer a lightweight and scalable screening tool that complements process-based atmospheric monitoring rather than replacing it.

Keywords International Wealth Index (IWI), NO_2 monitoring, Africa, Spatial autocorrelation, Machine learning in environmental policy

In pursuit of constantly improving socioeconomic conditions, countries that pledged emissions reductions under the Paris Agreement are, in aggregate, not on track to deliver them[1,2]. Holding those pledges to account requires knowing where emissions are produced and how that geography shifts as economies develop. No mechanism currently supplies that information systematically[3]. The accountability problem is in part an observational one.

The gases that matter most for those pledges are the hardest to trace to their emission locations. Carbon dioxide (CO_2) and methane (CH_4) remain in the atmosphere for years to millennia[4,5], so emissions from any single place register as a small excess above a large, well-mixed background[6,7]. Nitrogen dioxide (NO_2) behaves differently. Its daytime lifetime is a few hours, so it stays close to the places that emit it, and its column density, the amount of NO_2 in the air above a given point, varies sharply in space and time[8,9]. The Tropospheric Monitoring Instrument (TROPOMI) resolves those patterns globally, down to the urban scale[10,11]. NO_2 also harms health directly, with documented associations to respiratory and cardiovascular illness[12]. While it is not the gas the Paris Agreement governs, it may provide an indirect way of tracking part of the CO_2 variation.

Meanwhile, the socioeconomic processes that drive combustion are mapped in growing detail. Recently, gridded estimates of household wealth were developed, now covering Africa at 6.7 km resolution for the period

[1]Department of Computer Science and Engineering, Chalmers University of Technology, Gothenburg, Sweden. [2]AI and Global Development Laboratory, Linköping University, Linköping, Sweden. [3]Geomatics, Department of Environmental and Life Sciences, Karlstad University, Karlstad, Sweden. ✉email: fra.grieco@live.com

1990 to 2020[13,14]. With such socioeconomic data, we can now for the first time use a granular socioeconomic indicator, the International Wealth Index (IWI), to analyse how well it accounts for where satellite-observed NO_2 is high and where it is low.

Combustion releases NO_2 and CO_2 together, and across Africa the temporal correlation between them, computed month by month at each location, is moderate in magnitude yet positive and spatially organized (Fig. 5). We report that association as indicative context. A caveat: atmospheric-chemistry models represent sector- and fuel-specific co-emission ratios far more comprehensively than a probability-driven model does[15,16]. Thus, more research is needed to more accurately convert NO_2 observations into CO_2 emissions. The long-lived gases remain the quantities of ultimate interest, and extending this approach to them is open work.

We train a convolutional neural network (CNN) that takes gridded IWI as its only input and predicts TROPOMI NO_2 column density at locations the model never saw during training (Fig. 1). We extend the IWI series to cover 2019 to 2024, the years of complete TROPOMI coverage. Africa is the study area because the gridded IWI estimates are most extensive and reliable there[13]. IWI can also be projected forward, which permits an illustrative 2030 scenario that we present as a methodological demonstration that may help fully fledged forecasting methods.

The analysis is bounded. It relates one wealth index to one pollutant across one continent. It offers a lightweight screening tool for where emissions-generating activity concentrates. More work is required to produce process-based atmospheric models for emissions accounting.

Results

Predictive power of IWI on NO_2

Our model, a 3-layer convolutional neural network (CNN) shown in Fig. 1, predicted NO_2 column densities from IWI with an average accuracy of $R^2 = 0.56$. Fig. 2 shows how the model maps a patch of gridded IWI onto a patch of NO_2. We also evaluated alternative configurations, including deeper CNNs, VGG16-based models (VGG16 is a standard deep image-classification architecture), CNNs with wind data as an additional input, and conventional learners such as linear regression and random forest regressors (Fig. 6; see Methods). As Fig. 6 shows, the selected architecture reaches $R^2 = 0.57$, against 0.24 for the VGG16-based variant, 0.09 for linear regression, and −0.28 for the random forest. A negative value means the model predicts less well than the sample mean does. The ordering is therefore unambiguous, and the gap between the convolutional networks and the conventional learners is the largest single contrast in the comparison. We report that comparison descriptively by documenting the configurations explored, and we do not interpret the results as establishing general

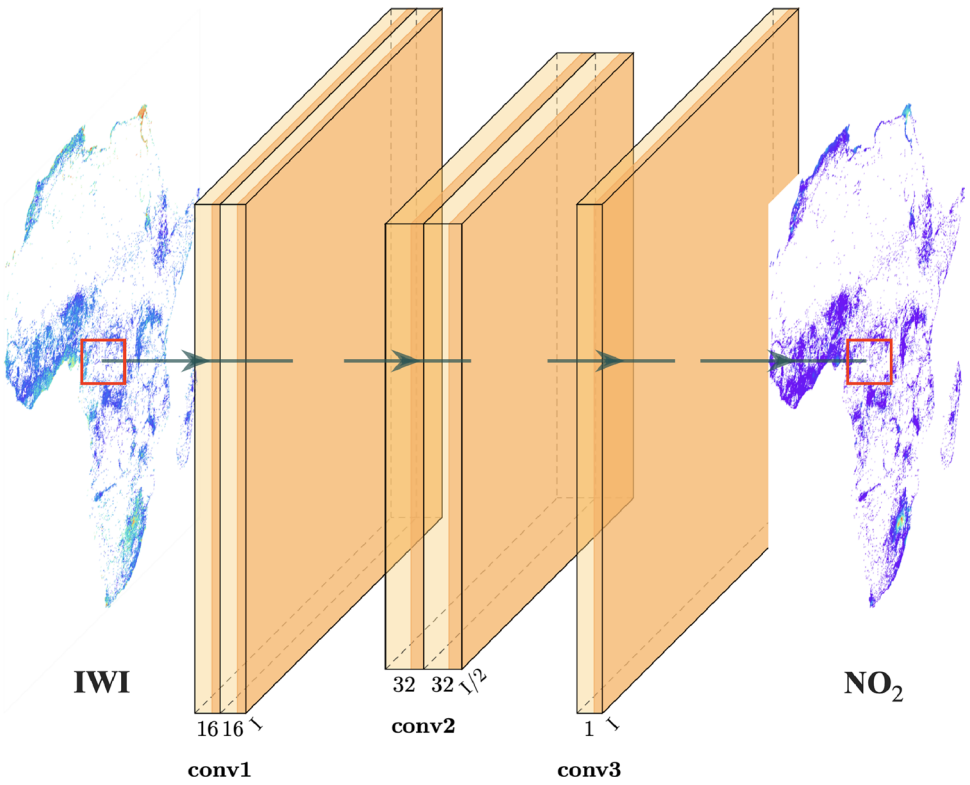


Fig. 1. Schematic representation of the CNN model used to predict NO_2 column densities from IWI data. The model processes gridded IWI input through multiple convolutional layers (conv1–conv3) to extract spatial features and generate NO_2 predictions at the same resolution. The numbers indicate the number of filters in each convolutional layer, while Roman numerals denote the corresponding downsampling factors.

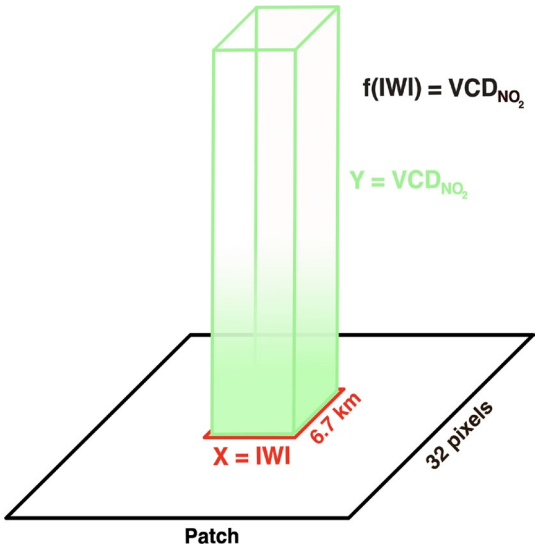


Fig. 2. Schematic representation of our model's framework.

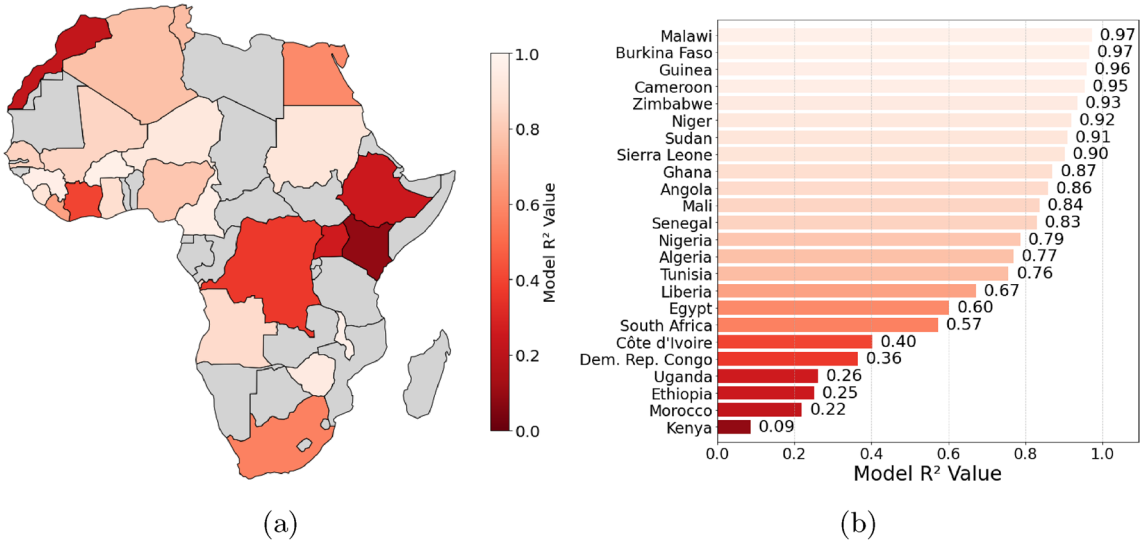


Fig. 3. Model performance (R^2) across African countries. R^2 values are obtained by training the model on the rest of the continent and using each country as a geographically isolated test dataset. Lighter shades indicate higher R^2 values, while grey regions represent countries with insufficient or missing data.

architectural superiority across deep learning models. Such a general claim would require benchmarking many models designed for that purpose.

Figure 3 shows the model's predictive performance across African countries, measured by the R^2 value obtained when each country in turn is used as a geographically isolated test dataset and the rest of the continent as training data, so that no data from the country being predicted entered its own training set. Lighter shades indicate higher predictive accuracy. Grey regions denote countries for which data were insufficient or not included in the analysis. The model reads the IWI map in square patches of 32×32 pixels (Fig. 2). In some countries, many of those patches were empty, because IWI predictions are missing in certain areas (see the white regions in Fig. 4, for example). We therefore considered only patches in which at least 50% of the pixels carry an IWI value, mainly because the datasets differ in resolution. As a result, we excluded countries with sparse IWI predictions from this study. Although some of these countries show a high correlation between CO_2 and NO_2, the limited availability of IWI data prevents their effective use in our deep learning models.

Countries such as Kenya, Ethiopia, Uganda, and the Democratic Republic of the Congo show lower R^2 values (darker red). This suggests that the model struggles to generalize well in these regions. Conversely, countries such as Burkina Faso, Mali, Niger, and Sudan show higher R^2 values (lighter shades), as do other parts of West Africa and the Sahel. Across the countries retained in the analysis, performance spans almost the full range of

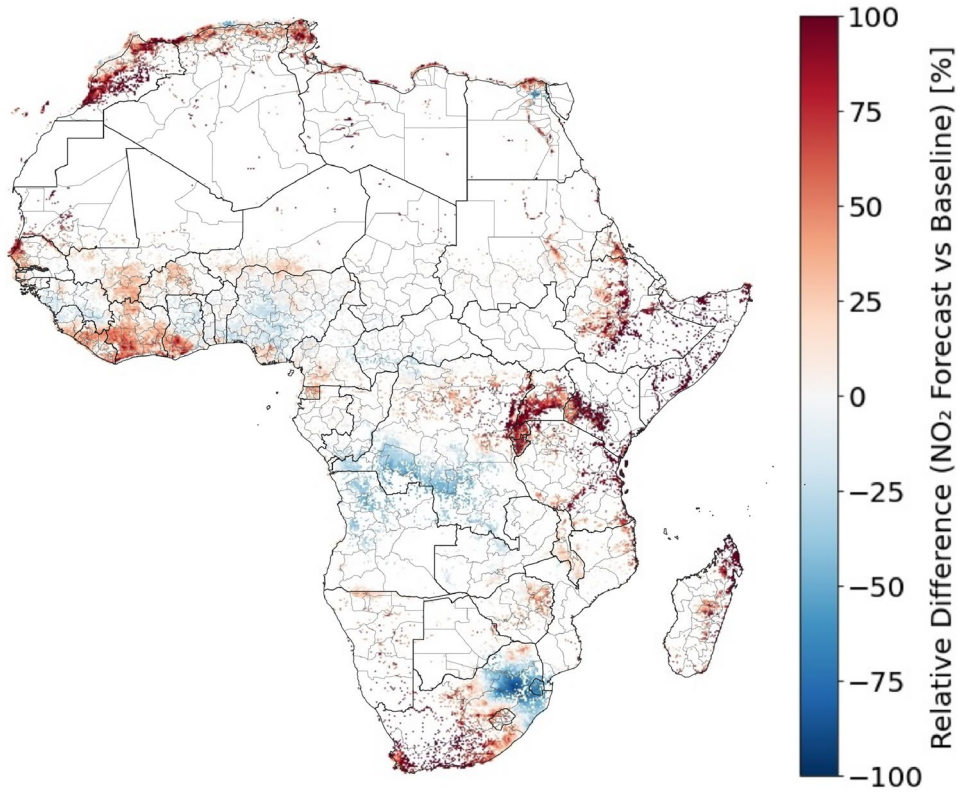


Fig. 4. Change in NO_2 column densities between 2019 and the projected 2030, over the populated areas of the African continent. First-level administrative boundaries (geoBoundaries Comprehensive Global Administrative Zones), with country outlines dissolved from the same units, are overlaid to locate the clustered changes.

the scale, and its geography is systematic rather than random: the weakest values concentrate in equatorial East Africa, while the strongest lie in the Sahel and West Africa. The Sahara itself is mixed, with Algeria among the stronger countries and Morocco among the weakest, so the pattern does not reduce to a simple arid-versus-humid contrast. Countries shown in grey carry no value at all: sparse IWI coverage kept them out of the analysis, so the grey is not a verdict on how the model performs there. Readers should keep those exclusions in mind when reading the map, because the excluded countries are themselves spatially clustered.

To explore why model performance (R^2) varied across countries, we regressed the country-level R^2 values against socioeconomic and governance indicators from the Quality of Government (QoG) dataset[17]. The selected structural and governance indicators explain cross-country variation in model performance well, with an uncentered R^2 (a fit statistic for a model without an intercept) of 0.89 and a highly significant overall model fit ($p < 0.001$). Perceived corruption is the only statistically significant predictor ($p = 0.007$), and its relationship with model performance is positive. Because the index scores higher where corruption is perceived to be lower, this result suggests that countries with lower levels of corruption tend to achieve higher predictive accuracy. In contrast, indicators such as government effectiveness, electricity access, and urbanization show weak or statistically insignificant associations once the other variables are controlled for (see Table 2a in the Appendix).

Intra-country projected changes in NO_2 column densities

Figure 4 illustrates the differences in NO_2 column densities between 2030 projections and 2019 observations from TROPOMI. To generate these projections, we first obtained IWI estimates from an Earth Observation–Machine Learning (EO-ML) method, which provides gridded socioeconomic data at a 6.7 km resolution for Africa from 1990 to 2020[13,14], extended by us to 2024 (see Methods). We then extended this series by linearly extrapolating IWI values to 2030. We fed these projected IWI values into our trained model, which predicted NO_2 column densities at the same spatial resolution. We then compared the model's 2030 output with the 2019 NO_2 column densities observed by TROPOMI to quantify changes over time and to identify regions with notable increases or decreases in emissions.

The map shows both increases and decreases in column densities across the African continent, and the predicted changes vary considerably within countries. Hotspots of increased column densities appear prominently in rapidly urbanizing and industrializing regions, such as East Africa (notably Kenya and Ethiopia), Central Africa, and parts of West Africa. Urban expansion, industrial growth, and the associated rise in transportation activities likely drive these increases. For instance, Kenya's industrialization efforts and Ethiopia's rapid urbanization align with these predictions, as seen in their urban development policies and economic

growth targets[18,19]. These regions are also particularly susceptible to rising emissions, because air quality control measures there are limited[20]. Predicted decreases in NO_2 column densities concentrate in parts of Southern Africa and localized areas in the Sahel region. These decreases may reflect a combination of socioeconomic transitions, shifts in energy sources, and emission control policies[21]. For example, South Africa's Nationally Determined Contribution (NDC) commits to transitioning away from coal-fired power plants and adopting renewable energy sources, which likely contributes to reduced emissions[22]. In the Sahel, sustainable agriculture and clean energy have spread, which reduces reliance on traditional biomass fuels and mitigates emissions from rural areas[23].

Interpreting these clustered patterns with respect to administrative units requires care about the resolution at which the model was validated. The validation design establishes reliability at country level (Fig. 3), and country level is therefore the main resolution it supports. The contextual NO_2–CO_2 association, by contrast, varies considerably within countries: across 707 first-level administrative units in Africa (provinces and their equivalents), the mean pixel-wise correlation ranges from −0.16 to 0.58, and within the median country the gap between the highest and the lowest unit is 0.18, with Mali's gap reaching 0.53. A country average would thus conceal substantial variation inside countries. We draw administrative boundaries on Fig. 4 so that readers can locate the clustered changes against the units they fall within. We accordingly read Fig. 4 at country level and treat the intra-country structure as descriptive: it indicates where projected changes concentrate, but we do not attach subnational reliability claims to it, because the held-out evaluation was not performed at that level. Countries with low country-level R^2 in Fig. 3, notably Kenya, Morocco, Ethiopia, Uganda and the Democratic Republic of the Congo, should correspondingly be read with greater caution in Fig. 4. Extending the validation design itself to administrative units is a natural next step, but it requires held-out evaluation at that resolution rather than reinterpretation of country-level results.

The Appendix (Fig. 7) compares the projected 2030 changes with the relative reduction targets declared in national NDCs. We present that comparison as exploratory. The quantity projected by the model is a change in atmospheric NO_2 column density, whereas NDC targets are generally expressed as economy-wide CO_2-equivalent reductions against country-specific baselines and sectoral scopes. Both sides can be written as percentages, but they are not commensurate quantities, and we therefore draw no compliance conclusions from the comparison.

Relationship between NO_2 and CO_2

Using monthly datasets of CO_2 and NO_2, we computed the temporal correlation between the two series at every grid cell worldwide. The resulting map shows where the two gases vary together over time. The NO_2 data, derived from the TROPOMI instrument, are available from 28 June 2018 onward, while the CO_2 dataset spans from January 2015 to February 2022. The two datasets overlap for 43 months, a sample large enough to capture seasonal variability and to assess temporal correlations at monthly resolution.

Figure 5 presents the resulting global correlation map. The correlation coefficients are far from randomly scattered: they form distinct regional patterns in the relationship between CO_2 and NO_2. Correlations are strongly positive over regions such as Africa, South Asia, and parts of South America. This pattern indicates that, in these regions, common emission sources and processes largely control both gases. Dominant contributors include biomass burning (e.g., savanna fires, deforestation, and agricultural burning), as well as rapidly growing urban and industrial emissions. These sources emit CO_2 and NO_2 at the same time, so the two gases rise and fall together from month to month, which produces high positive correlations at the monthly scale.

To characterize this spatial structure formally, we computed global Moran's I on the mapped correlation coefficients. Moran's I measures whether neighbouring cells carry similar values, and it is therefore a statistic about the map rather than about the two gases. The global value is $I = 0.95$ and the Africa-only value is $I = 0.94$, with pseudo $p = 0.001$ in both cases (row-standardized eight-neighbour grid adjacency, 999 permutations); no permutation of the observed coefficients reproduced a comparable degree of clustering. The mapped correlations are thus organized into coherent regions rather than distributed as spatial noise. The magnitude of the association is nevertheless modest: the mean coefficient across Africa is 0.13, and 51 of 54 African countries have a positive country mean. The pattern is best described as moderate in magnitude but spatially consistent.

Seasonality contributes to this structure. In dry seasons, more fires burn and both CO_2 and NO_2 rise together; in wet seasons, less burning takes place and both fall together. Because both gases have pronounced annual cycles whose amplitude and phase vary with latitude, part of the mapped correlation reflects shared seasonality rather than a shared source: latitude band alone accounts for approximately 74% of the variance in the global field, but only 49% within Africa. We therefore treat the mapped correlation as indicative context for the African analysis. It does not establish a deterministic relationship between the two gases, and we do not use it to convert NO_2 observations into CO_2 quantities.

In contrast, regions such as Europe and Canada exhibit weak, near-zero, or even negative correlations. These weak correlations reflect a decoupling between CO_2 and NO_2, because different processes now dominate each gas. Over these regions, NO_2 emissions have fallen sharply over time under stringent air quality regulations, including vehicle emission standards and industrial controls. CO_2 concentrations, meanwhile, have not fallen proportionally, because they reflect long atmospheric lifetimes and cumulative global emissions.

Overall, the correlation patterns vary from region to region, so the relationship between CO_2 and NO_2 is strongly region-dependent. We therefore treat NO_2 as informative about combustion-related CO_2 activity only in regions where common emission sources appear to govern both species and where the two vary together over time. Africa is comparatively favourable in this respect: 91.6% of African grid cells show a positive coefficient, against 58.8% globally. This observation motivates the geographic scope of this study, but it is a statement about context rather than evidence for the predictive model, which relates IWI to NO_2 via deep learning; the spatial correlation between NO_2 and CO_2 is a separate, contextual analysis.

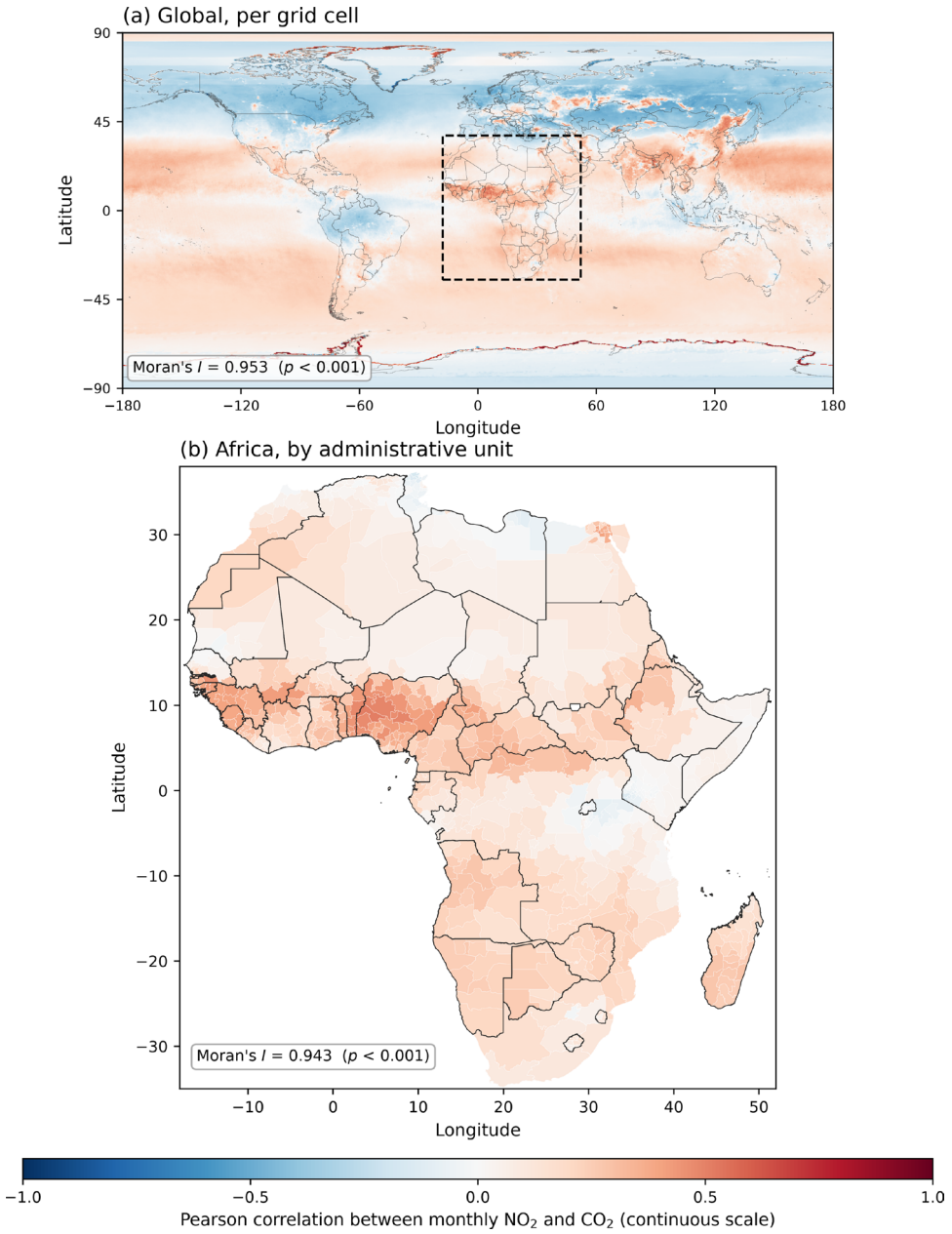


Fig. 5. Pearson correlation between monthly CO_2 and NO_2, June 2018 to February 2022. At each grid cell the coefficient correlates the two monthly series at that location over time, so it is a temporal statistic displayed spatially. (**a**) Global field, one value per grid cell. (b) Africa, the same coefficients averaged within first-level administrative units ($n = 707$, geoBoundaries). One continuous scale spans −1 to 1; panel (**b**) is pale because the administrative means are genuinely small, from −0.16 to 0.58. Global Moran's $I = 0.95$ and Africa-only $I = 0.94$ (row-standardized eight-neighbour adjacency, 999 permutations, seed 20260810, pseudo $p = 0.001$), computed at 0.50°. Moran's I describes clustering in the mapped coefficients; it does not establish common sources, causal coupling, or the validity of the IWI-to-NO_2 model.

Discussion

This study examines the predictive power of a key socioeconomic indicator, the International Wealth Index (IWI), for NO_2 column densities across Africa. By analysing the spatial variation in the temporal correlation between CO_2 and NO_2, we characterize where the two gases co-vary. That association is moderate in magnitude but spatially organized, and it is most consistently positive across Africa, where the two gases are frequently co-emitted, because emission controls are less stringent and traditional combustion is common. In regions such as Europe, by contrast, the two pollutants have decoupled. We treat the mapped association as indicative context, not as a basis for converting NO_2 observations into CO_2 quantities. Linking IWI with satellite-derived NO_2 data provides a lightweight screening tool for relating development patterns to observed pollutant levels and for

identifying where further monitoring may be warranted. To keep large-scale analyses computationally efficient, we used a 3-layer CNN, which offers robust predictive performance.

The predictive power of IWI is particularly evident across the African continent, where IWI is a useful proxy for socioeconomic drivers of emissions, including urbanization, infrastructure development, and economic activity. However, this relationship depends inherently on development policies. If future policy shifts in African countries lead to reduced co-emission of CO_2 and NO_2, the observed predictive strength would likely change accordingly.

Predictive accuracy does not imply causation. Our findings show that IWI is useful for capturing spatial patterns in NO_2 column densities, but future research should focus on establishing causal links between specific socioeconomic activities and NO_2 emissions. In particular, separating contributions from transportation, industrial processes, and residential energy use could provide more directly usable guidance for policymakers.

Intra-country and regional insights

The spatially resolved predictions from our model reveal considerable intra-country variability in NO_2 column densities. Hotspots of increased column densities appear prominently in rapidly urbanizing and industrializing regions, such as Kenya and Ethiopia in East Africa, as well as parts of Central and West Africa. These findings align with documented trends in urban expansion and industrial growth, which drive transportation and energy demands[18,19].

Conversely, predicted decreases in column density appear in Southern Africa and localized regions within the Sahel. These reductions may reflect shifts in socioeconomic activities, transitions to cleaner energy sources, and the implementation of emission control policies[21,23]. For example, South Africa's commitment to phasing out coal-fired power plants and the adoption of sustainable agriculture in the Sahel region have likely contributed to these trends[20,22].

Designing targeted interventions requires forecasts of how socioeconomic changes will influence column densities at the local level, particularly where air quality control measures or institutional capacity are limited.

To investigate the variability in model performance across countries, we regressed the country-level R^2 values against selected socioeconomic and governance indicators from the QoG time-series dataset[17]. The analysis explained a substantial portion of the cross-country variability, and corruption perception was the only significant predictor. This result suggests that stronger institutional quality and lower corruption are associated with higher model accuracy. Other factors such as GDP per capita, urbanization, and electricity access showed weaker associations.

Relation to declared NDC targets

The Appendix reports an exploratory comparison between the projected 2030 change in NO_2 column density and the relative reduction targets declared in national NDCs. We refrain from drawing compliance conclusions from it. The two sides of that comparison are not commensurate: the model projects a change in an atmospheric column density, while NDC targets are generally economy-wide CO_2-equivalent reductions defined against country-specific baselines and sectoral scopes.

Establishing a mechanistic link would require more research: a validated transformation from observed NO_2 column densities to emissions of the gases that NDCs actually govern, including CO_2. That is a substantial undertaking in its own right, involving combustion-specific emission ratios, atmospheric chemistry, and transport, and we identify it below as the necessary next step. Our empirical analysis indicates that part of the CO_2 variation is likely linked to NO_2 emissions in neighbourhoods where socioeconomic conditions also vary.

Advancing emissions monitoring

Integrating IWI with satellite-derived NO_2 column densities advances emissions monitoring. Unlike traditional methods that rely on self-reported inventories, our approach provides an independent, high-resolution assessment of emission trends. Because NO_2 is short-lived and present at ground level, our framework can identify emission sources and hotspots at the resolution of the gridded IWI input.

Intra-country variation in column densities may inform subnational policy interventions. For instance, targeting specific urban centres or industrial zones identified as emission hotspots can maximize the impact of mitigation strategies. Our model can also support scenario-based analyses, so policymakers can assess the implications of various socioeconomic trajectories for future emissions.

Limitations and future directions

This study has several limitations. Predictive models carry uncertainty, particularly in regions with sparse data or unusual emission patterns; countries with lower model performance, such as Kenya and Ethiopia, may need additional data or context-specific adjustment. The contextual correlation analysis carries its own caveat: the CO_2 field is a model assimilation product, in which satellite retrievals are blended into an atmospheric transport model, so part of its spatial smoothness, and hence the high Moran's I, reflects the assimilation system rather than the atmosphere.

We addressed sampling-related uncertainty with cross-validation over 1000 random training-validation-test splits, and probed sensitivity to the input patch size and to the network architecture, comparing the selected model against VGG16-based CNNs, random forest regressors, and linear models (Table 1, Fig. 6).

Three substantive gaps remain. First, our projections do not separate NO_2 by emission sector, so the aggregated changes cannot isolate sector-specific trends even though mitigation strategies differ across transport, industry, power generation, and residential combustion[24]. Second, the African focus, justified by the quality of the available IWI estimates, leaves transferability untested: the way wealth couples to emissions differs across regions, rising with cleaner technology in high-income settings but with fossil-fuel-intensive industrialization elsewhere. Third,

Patch size	Depth	Filters	Inputs	R^2	R^2_0	% p-values < 0.05
32	2	8	IWI	0.20 ± 0.34	−0.04 ± 0.12	30%
			IWI, wind	0.29 ± 0.27	0.03 ± 0.12	40%
		16	IWI	0.37 ± 0.38	0.24 ± 0.19	50%
			IWI, wind	0.34 ± 0.32	0.10 ± 0.15	40%
	3	16	IWI	0.51 ± 0.2	−0.10 ± 0.12	50%
			IWI, wind	0.50 ± 0.23	−0.10 ± 0.16	60%
		32	**IWI**	**0.57 (0.56 ± 0.12)**	**−0.06 (−0.01 ± 0.18)**	**80% (69.7%)**
			IWI, wind	0.53 ± 0.20	−0.15 ± 0.14	70%
16	2	8	IWI	−0.14 ± 0.61	−0.17 ± 0.18	10%
			IWI, wind	−0.13 ± 0.50	−0.23 ± 0.18	20%
		16	IWI	−0.11 ± 0.63	0.03 ± 0.22	10%
			IWI, wind	−0.10 ± 0.53	−0.02 ± 0.11	20%
	3	16	IWI	0.18 ± 0.33	0.03 ± 0.11	30%
			IWI, wind	0.12 ± 0.37	−0.26 ± 0.11	20%
		32	IWI	0.14 ± 0.41	−0.20 ± 0.22	30%
			IWI, wind	0.14 ± 0.41	−0.10 ± 0.19	30%

Table 1. Performance comparison of various CNN configurations. Bold values indicate the best-performing model configuration. The values in parentheses correspond to those obtained over 1000 different training-validation-test splits.

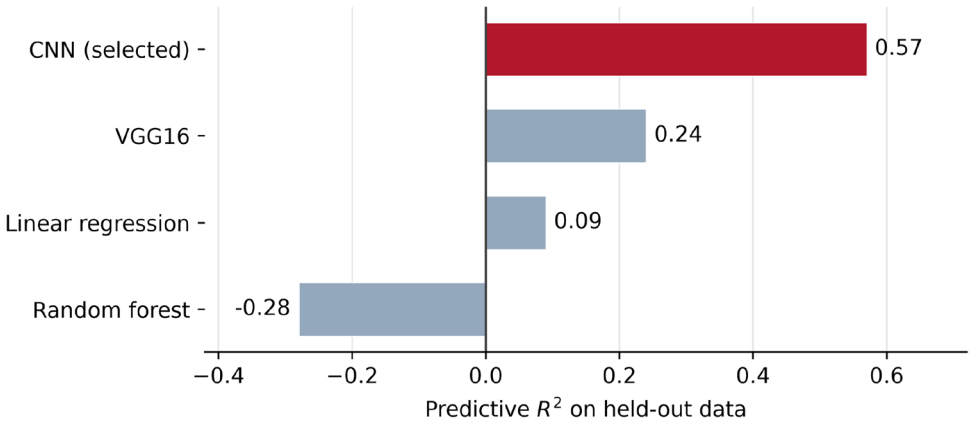


Fig. 6. Predictive performance of the model families examined, as mean R^2 on held-out data over 10 training-validation-test splits. Negative values indicate performance worse than predicting the sample mean. The selected convolutional neural network is shown in red. We report R^2, the directly interpretable measure of predictive accuracy, for each model family. Configuration-level benchmarks for the selected architecture, including a shuffled-target null and the proportion of splits reaching significance, are reported in Table 1.

the strength of the NO_2–CO_2 relationship depends on the dominant sectors and regional energy profiles; it is relatively stable for transport and industrial combustion[25] but weakens or decouples for power generation shifting to cleaner fuels, residential biomass burning, and agriculture[26].

The most consequential direction for any policy-facing use is a mechanistic rather than statistical link between the two gases. A correlation coefficient cannot by itself carry an emissions attribution, because the mapping from an NO_2 column density to a CO_2 emission rate depends on combustion conditions, fuel type, plume age, and atmospheric chemistry. Our own results make this concrete: across 707 first-level administrative units in Africa the mean correlation ranges from −0.16 to 0.58, so no single conversion factor would apply continent-wide. A physically grounded transformation, built from combustion emission factors and NO_x lifetime, constrained by atmospheric transport and validated against independent inventories, would be required; biomass-burning regions, where a single fire emits CO_2 through complete combustion and NO_x through incomplete combustion, are the natural setting in which to attempt it. Alongside this, future work could integrate sectoral attribution, combine multi-pollutant observations of NO_2, CO_2, and CH_4, and test the framework in other regions to establish where it generalizes.

Methods

Data description

International wealth index (IWI)

The International Wealth Index (IWI) is an asset-based measure of material well-being designed for comparability across low- and middle-income countries. Unlike other wealth indices, which are often country-specific and context-bound, IWI applies one standard scale to household wealth and socioeconomic status, so it supports comparisons across countries and over time. Developed using data from 2.1 million households across 97 countries, IWI is grounded in household asset ownership, access to basic services, and housing quality, and it captures material well-being on a global scale.

IWI evaluates a household's material standard of living using a set of assets, including consumer durables such as televisions, refrigerators, and bicycles; housing characteristics such as the quality of flooring and toilet facilities; and access to essential utilities such as electricity and clean water. Principal Component Analysis (PCA) assigns each asset a weight according to its contribution to overall wealth. These weights are combined into a unified scale that runs from 0 to 100, where a score of 0 represents a household with no durable goods, poor-quality housing, and no access to utilities, and 100 represents a household possessing all assets and services included in the index[27].

The IWI is available only at the locations and times where household surveys have been conducted. To overcome this limitation[13], developed an EO-ML method to infer neighbourhood-level material-asset wealth across the populated areas of the African continent from 1990 to 2020[14]. This method combines multi-temporal satellite imagery, available Demographic and Health Surveys (DHS), and recurrent convolutional neural networks to produce spatially and temporally consistent estimates of IWI. For this study, we applied their model to obtain data for more recent years, generating annual IWI data covering 2019 to 2024 to align with the operational period of the TROPOMI instrument. The resulting data are organized into gridded raster images covering all populated areas of Africa. Each grid cell measures 6.72 × 6.72 km, a spatial scale derived from the CNN input size of 224 × 224 pixels and the native Landsat resolution of 30 m/pixel used in[13]. For each cell, the model predicts a single IWI score, the mean material-asset wealth of the corresponding neighbourhood. It draws on multi-temporal sequences of multispectral Landsat imagery, including red, green, blue, near-infrared, shortwave infrared, and thermal bands, augmented with nighttime luminosity data from the Defense Meteorological Satellite Program (DMSP) and Visible Infrared Imaging Radiometer Suite (VIIRS) satellites, all processed via Google Earth Engine. The model assigns predictions only to populated cells; uninhabited areas are excluded. This spatially explicit raster of annual IWI values is the single-channel input to our CNN model.

This study focuses on Africa as a case study because[13] provide reliable IWI estimates for this region, offering a geographically extensive and temporally consistent dataset to validate our methodology. The focus on the African continent is not intended to disproportionately scrutinize countries that are less responsible for climate change. Instead, we use the available high-quality socioeconomic data to demonstrate the broader applicability of our approach in regions with reliable information.

CO_2data We obtained atmospheric carbon dioxide observations from the Orbiting Carbon Observatory-2 (OCO-2) mission. Launched in 2014, OCO-2 is a sun-synchronous satellite designed to provide high-resolution measurements of the column-averaged dry air mole fraction of carbon dioxide (X_{CO_2}), the average CO_2 concentration through the air column, with a precision of approximately 1 ppm. The instrument uses a three-channel grating spectrometer to measure reflected sunlight in the molecular oxygen (O_2) A-band and two carbon dioxide (CO_2) bands[28].

For this study, we used the OCO-2 GEOS Level 3 monthly assimilated X_{CO_2} product (Version 10r) to provide a continuous global view of atmospheric carbon dioxide. The NASA Global Modeling and Assimilation Office (GMAO) produces the dataset with the Goddard Earth Observing System (GEOS) Constituent Data Assimilation System (CoDAS). This system synthesizes OCO-2 Level 2 X_{CO_2} retrievals with a high-resolution atmospheric transport model[29].

NO_2data Burning fossil fuels, such as those used in vehicles, power plants, and industrial activities, generates most nitrogen dioxide (NO_2). Natural sources such as soil microbial activity and vegetation contribute smaller amounts. Beyond its role as a direct pollutant, NO_2 is a precursor to other harmful atmospheric compounds, including ground-level ozone, fine particulate matter, and acid rain. Despite its significant health and environmental impacts, NO_2 is not categorized as a major greenhouse gas, because of its relatively low global column densities (approximately three orders of magnitude lower than carbon dioxide, CO_2) and its short atmospheric lifetime of a few hours to a day. That short lifetime keeps NO_2 concentrated near emission sources, so it is a valuable indicator for identifying pollution hotspots[30].

We use NO_2 measurements from the Tropospheric Monitoring Instrument (TROPOMI), a high-resolution spectrometer aboard the Sentinel-5P satellite, launched in 2017. TROPOMI captures NO_2 column densities with a spatial resolution as fine as 5.5 km × 3.5 km, so it can detect medium-scale pollution sources, including urban centres, industrial facilities, highways, and large individual emission events such as wildfires or shipping activities. TROPOMI observes at a fixed time of approximately 13:30 local solar time, which keeps measurements consistent and reduces variability caused by daily fluctuations in NO_2 column densities[31]. Extensive validation studies have confirmed the instrument's accuracy and reliability in monitoring atmospheric NO_2[32].

The instrument detects sunlight reflected from the Earth's surface and atmosphere, analysing a broad range of wavelengths, from ultraviolet to shortwave infrared. Through these measurements, TROPOMI identifies absorption features specific to NO_2 and estimates the tropospheric vertical column density (VCD) of the gas[33], that is, the amount of NO_2 standing above each unit of surface area up to the top of the troposphere. This quantity is a proxy for ground-level emissions. In fact, although minor amounts of NO_2 can be transported from the stratosphere via processes such as photolysis of nitrous oxide (N_2O) and subsequent stratospheric intrusions, their impact on tropospheric column densities is negligible compared to surface-level sources[34].

For this analysis, we used yearly medians of the NO_2 data from 2019, the first complete year of TROPOMI observations, through 2024. We re-gridded those medians to match the resolution of the IWI data.

Quality of government (QoG)
We complemented our analysis with country-level governance and socioeconomic indicators from the Quality of Government (QoG) Standard Time-Series Dataset (2025), compiled by the University of Gothenburg. The dataset aggregates annually updated variables from multiple reputable sources, including the World Bank, Transparency International, and the World Justice Project, and provides globally comparable measures of institutional quality, governance performance, and development outcomes. From this dataset, we extracted indicators such as GDP per capita, industrial share, urban population, government effectiveness, rule of law, corruption perception, and electricity access[17]. We used these variables to investigate which structural and institutional factors might explain the cross-country variability in model performance (R^2).

Temporal correlation and spatial autocorrelation

The contextual analysis in Fig. 5 involves two distinct statistics, computed in sequence.

First, at each eligible grid cell j, we calculate Pearson's correlation coefficient across the months with valid paired observations:

$$r_j = \frac{\sum_{t\in\mathcal{T}_j}(x_{jt}-\bar{x}_j)(z_{jt}-\bar{z}_j)}{\sqrt{\sum_{t\in\mathcal{T}_j}(x_{jt}-\bar{x}_j)^2}\sqrt{\sum_{t\in\mathcal{T}_j}(z_{jt}-\bar{z}_j)^2}}, \tag{1}$$

where x_{jt} and z_{jt} denote CO_2 and NO_2 respectively at cell j in month t, and $\mathcal{T}_j$ is the set of months with valid paired observations at that cell. Each r_j is therefore a temporal statistic computed independently at a single location; the map in Fig. 5 displays those values spatially but does not pool them.

Second, we summarize spatial autocorrelation in the resulting field of r_j values with the global Moran statistic:

$$I = \frac{N}{S_0}\frac{\sum_i\sum_j w_{ij}(r_i-\bar{r})(r_j-\bar{r})}{\sum_i(r_i-\bar{r})^2}, \qquad S_0 = \sum_i\sum_j w_{ij}, \tag{2}$$

where w_{ij} is the spatial weight linking cells and j, and N is the number of eligible cells. We use row-standardized eight-neighbour (queen) grid adjacency, so that $S_0 = N$. We assess statistical significance by permutation: we hold the grid and the neighbourhood structure fixed, randomly reassign the observed coefficients among eligible cells, and recompute I. We use 999 permutations and a fixed random seed of 20260810, and report the pseudo p -value $(1 + m)/(1 + 999)$, where m is the number of permutations attaining at least the observed value.

The correlation raster is stored at approximately 1 km resolution, which is finer than the native spatial support of the assimilated CO_2 product (roughly $0.5^\circ \times 0.625^\circ$). Because Moran's I computed on an oversampled field is inflated by resampling rather than by geophysical structure, we block-average the coefficients to 0.5031° , referred to as 0.50° in the caption of Fig. 5, before computing the statistic, requiring at least 50% valid native cells per aggregated cell, and verify that conclusions are unchanged at 0.2515°. We report one global value and one Africa-only value, and do not compute local indicators of spatial association, alternative weight matrices, or block bootstraps.

We computed country-level and first-level administrative summaries of the correlation field by averaging the same raster within each unit, using Natural Earth country boundaries and geoBoundaries Comprehensive Global Administrative Zones respectively.

NDC data harmonization

Nationally Determined Contributions (NDCs) are central to the Paris Agreement's objective of limiting global temperature rise to well below 2 C above pre-industrial levels, with efforts to cap the increase at 1.5 C. Each signatory nation must formulate, communicate, and maintain successive NDCs that detail its strategies for reducing greenhouse gas emissions and adapting to climate change impacts. NDCs embody the global commitment to combat climate change, with each country contributing according to its capabilities and responsibilities. By publicly outlining their climate actions, countries provide a basis for tracking progress[35].

Countries publish their emission reduction targets for various GHGs, summarized as CO_2 equivalents (CO_2e), for different target years and relative to different base years. This variability complicates direct comparisons between countries. Additionally, NDCs follow no common template: countries present them as separate documents in varying formats. Some NDCs include detailed sector-specific breakdowns and distinctions between conditional (dependent on external support, such as funding or technology transfer) and unconditional (self-financed or guaranteed) commitments. Others only specify an aggregate reduction target without elaborating on the methods or conditions for achieving it[36].

To address these inconsistencies, we standardized all NDCs by converting them to a common baseline year (2019, the first full year of TROPOMI observations used in this study) and a common forecast year (2030). The conversion required linearly interpolating or extrapolating data from the reference years provided in the NDCs. We then calculated the difference in total CO_2 equivalent emissions between 2019 and 2030 for each country. Where available, we prioritized conditional targets to reflect the maximum commitments pledged. However, we excluded countries that report their reductions only relative to a Business-As-Usual (BAU) scenario for their estimation year, because those targets cannot be compared directly within this framework.

These results require cautious interpretation, because the standardization process introduces uncertainties. We assume linear emission trajectories between base years and target years, a simplification that may not reflect the complex, sector-specific dynamics of emission reduction efforts.

Model architecture and training

The primary model used in this study is a 3-layer convolutional neural network (CNN) (see Fig. 1). The model takes as input patches of 32×32 pixels, square subregions of the gridded maps, each carrying a single channel of IWI values, and it takes the corresponding NO_2 patches as targets. We created the patches by dividing the IWI and NO_2 images from each year into smaller regions, so that each training example carries the spatial context around a location rather than a single cell, and we augmented them through rotation, flipping, and striding.

The first layer applies a set of 16 convolutional filters, each with a kernel size of 3×3, extracting spatial features while preserving the input dimensions through "same" padding. A 2×2 max pooling layer then reduces the spatial dimensions of the feature maps. This pooling step helps the model capture lower-resolution representations of the input while reducing computational complexity. To mitigate overfitting, a dropout layer after pooling randomly deactivates 25% of the neurons during training.

A second convolutional layer then applies 32 filters with the same kernel size of 3×3, rectified linear unit (ReLU) activation, and "same" padding. An upsampling operation restores the spatial dimensions of that output to their original size. Finally, the output layer produces a single-channel result using a 3×3 convolutional filter with ReLU activation, so the predicted patch matches the input dimensions.

We trained the model with the Adam optimizer and a custom loss function that handles missing values through a masked mean squared error, so that cells without data do not contribute to the loss. We processed 32×32 patches in batches of 1000 and trained over 10 epochs. Test data comprised 20% of the total available patches, randomly split from the dataset. To prevent leakage between training and test data, we isolated the test dataset geographically, so that no patches from the same region entered both the training and test sets, even when they came from images taken in different years.

We selected this architecture after testing multiple configurations, including CNNs of various depths and with varying numbers of convolutional filters, VGG16-based models, random forest regressors, and other CNN models incorporating additional input variables such as wind data from ERA5, the global climate reanalysis dataset produced by the European Centre for Medium-Range Weather Forecasts (ECMWF). Table 1 and Fig. 6 summarize those configurations. We considered incorporating wind as an additional input because wind influences the dispersion and transport of NO_2, affecting observed column densities independently of emission rates. However, adding wind did not improve predictive performance. This suggests that the NO_2–IWI relationship is robust even without accounting for wind variability. Among the CNN configurations in Table 1, the non-selected settings show a lower proportion of p-values below 0.05 than the chosen configuration. We do not compare dispersion across rows, because the spread reported for the selected configuration is computed over 1000 splits while the others are over 10. We report this as a description of the configurations tested here, and not as evidence of general architectural superiority. CNN configurations with patch sizes smaller or larger than those presented in Table 1 performed worse. Models with smaller patch sizes often failed to converge, while those with larger patches had R_0^2 values comparable to R^2, so they carried no meaningful predictive power.

Table 1 shows that the best-performing model is a CNN with a patch size of 32 pixels, 3 layers, 32 filters, and IWI as the sole input. This model achieves an R^2 of 0.57, an R_0^2 of −0.06, and 80% of p-values below 0.05.

For each model, we computed R^2 values over 10 different training-validation-test splits of the data, and the table reports the mean of these R^2 scores across the 10 splits. R_0^2 represents the average R^2 obtained by training models on shuffled NO_2 data (i.e., randomizing the target variable). This process destroys meaningful relationships, and values close to 0 are expected, indicating poor performance. Specifically, for each training-validation-test split, we shuffled the NO_2 images 10 different times and trained a model on each shuffled dataset. The reported R_0^2 value is the mean over all these shuffled cases. Comparing R^2 with R_0^2 shows how much better the model performs relative to a random baseline. The percentage of p-values below 0.05 represents the proportion of splits where the model's performance was statistically significant compared to the benchmark R_0^2. A p-value below 0.05 indicates that the model's performance is unlikely to have occurred by chance. A higher percentage here signifies more consistent and reliable model performance across the different data splits.

To ensure the robustness of our results, we trained the best-performing configuration on 1000 different training-validation-test splits. For each split, we shuffled the NO_2 images 100 times to calculate the benchmark R_0^2. Across these splits, the model achieved an R^2 of 0.56, an R_0^2 of −0.01, and a p-value below 0.05 in 69.7% of cases compared to the random-shuffling benchmark (values in parentheses in Table 1).

Scenario modelling and forecasting

To project NO_2 column densities in 2030, a year widely used as a benchmark for emission reduction commitments in international agreements, we fitted a linear trend to the IWI data over time for each pixel. The combined series spans 1990 to 2024, and we used that trend to extrapolate IWI values for 2030, which we then fed into our trained model to predict future NO_2 column densities. We chose this method for its simplicity; it estimates NO_2 column densities under a scenario where socioeconomic trends continue along their historical trajectory.

For country-level column densities in 2030, we aggregated predicted NO_2 column densities across all pixels corresponding to populated areas, i.e., those where IWI data were available. We then computed the change in column densities between 2019 (from TROPOMI observations) and 2030 (model predictions) for each country. To quantify uncertainties in the column density predictions, we propagated errors from two main sources: uncertainties in the linear regression parameters used to project IWI forward in time and the measurement uncertainty of TROPOMI NO_2 observations in 2019.

We compared these changes in NO_2 column densities between 2019 and 2030 directly with the change in Nationally Determined Contributions (NDCs) for total greenhouse gas (GHG) emissions, reported in CO_2 equivalents (CO_2e).

For the purpose of the exploratory NDC comparison, this approach assumes that NO_2 column densities are strongly correlated with emissions of other GHGs, particularly CO_2, because the two share emission sources in human activities such as industrial processes, transportation, and energy production. NO_2 is co-emitted with CO_2 in combustion and industrial activities, so it is a useful proxy for tracking broader pollutant emissions. Prior research has demonstrated the viability of using NO_2 as an estimator of CO_2 emissions[37].

However, this approach has inherent limitations. Emission ratios between NO_2 and other pollutants can vary across sectors and regions because fuel types, combustion efficiencies, and pollution-control technologies differ. NO_2 provides a valuable spatial and temporal indicator of emission trends, but translating NO_2 variations directly into CO_2e reductions requires care. Further refinements, including sector-specific adjustments and additional environmental factors, could improve the accuracy of this projection framework.

Data availability

IWI estimates can be downloaded at https://dataverse.harvard.edu/dataset.xhtml?persistentId=doi:10.7910/DVN/9DINV4[38]; TROPOMI L2 data can be downloaded upon registration at https://disc.gsfc.nasa.gov/datasets/S5P_L2__NO2___HiR_2/summary?keywords=TROPOMI[39]; the Quality of Government (QoG) dataset can be downloaded at https://www.gu.se/en/quality-government/qog-data/data-downloads/standard-dataset[17].

Appendix: cross-country determinants of model performance

	coef	std err	z	P> |z|	[0.025	0.975]
wdi_gdpcappppcur	1.82e-05	2.66e-05	0.685	0.493	-3.39e-05	7.03e-05
wdi_gdpind	-0.0007	0.009	-0.073	0.941	-0.018	0.017
wdi_popurb	0.0041	0.006	0.683	0.495	-0.008	0.016
wbgi_gee	-0.2469	0.172	-1.438	0.151	-0.584	0.090
ti_cpi	0.0171	0.006	2.712	0.007	0.005	0.030
wdi_acel	-0.0059	0.005	-1.299	0.194	-0.015	0.003

Table 2. Ordinary least squares (OLS) regression results examining the relationship between model performance (R^2) and country-level socioeconomic and governance indicators. The table reports the estimated coefficients (coef), robust standard errors (std err), test statistics (z), and two-tailed significance levels (P> |z|), along with 95% confidence intervals ([0.025, 0.975]). Predictors include GDP per capita (wdi_gdpcappppp), industry share of GDP (wdi_gdpind), urban population share (wdi_popurb), government effectiveness (wbgi_gee), perceived corruption (ti_cpi; higher values indicate lower corruption), and electricity access (wdi_acel) from the Quality of Government (QoG) dataset[17]. The regression explains 89% of the variation in R^2 values across 23 African countries. Corruption is the only statistically significant predictor.

The comparison below is exploratory and is reported here rather than among the main results. As stated in the Discussion, a change in atmospheric NO_2 column density and an economy-wide CO_2-equivalent reduction target are not commensurate quantities, and no compliance conclusions follow from comparing them.

Exploratory comparison with NDC goals

The results show substantial discrepancies between the projected difference in NO_2 column densities for 2030 and the relative reduction targets outlined in the NDCs for many African countries. Figure 7a presents a histogram comparing the column density variation from 2019 to 2030 as projected by the model versus the NDC goals for each country.

For some countries, including Burkina Faso, Ghana, Liberia, Mali, Nigeria, and Tunisia, the projected change in column density is larger than the relative reduction declared in the NDC. For others, including Cameroon, Egypt, Guinea, and Malawi, the projected change is smaller. We describe these as differences between two percentages, and not as evidence that a country will or will not meet its commitments, because the two percentages refer to different underlying quantities.

Figure 7b displays the same comparison geographically. The larger gaps appear in parts of West Africa and the smaller gaps in parts of Southern Africa. Any interpretation of this pattern in terms of institutional capacity or policy effectiveness would require evidence that this analysis does not provide.

We retain this material because it documents an avenue that was examined and because a policy-facing reading was requested; the transformation required for any compliance reading is identified in the Discussion as future work.

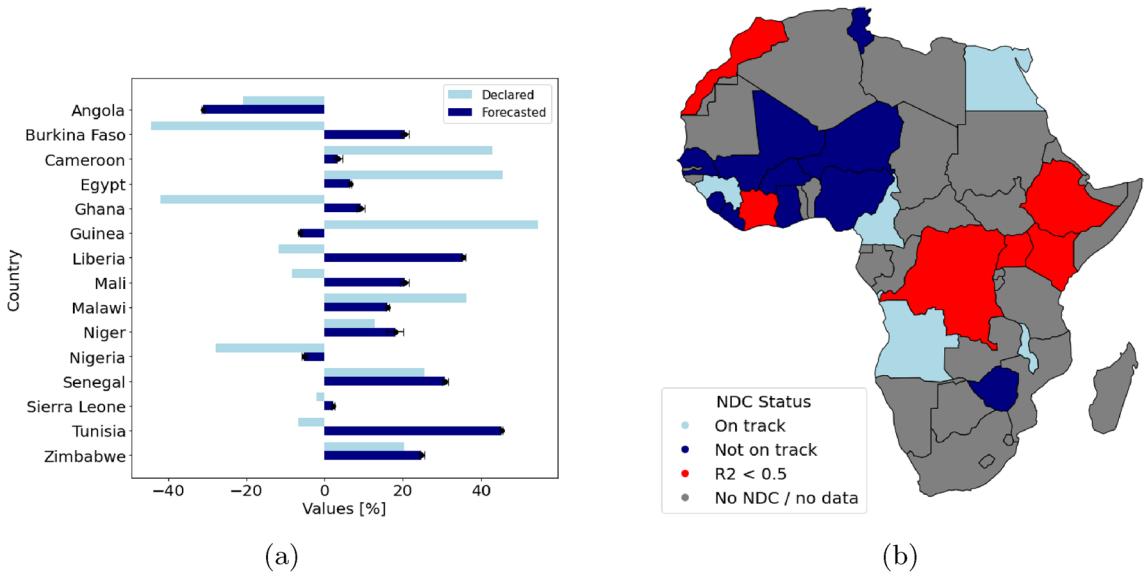


Fig. 7. (**a**) Histogram comparing NDC goals and predicted NO_2 column density variation between 2019 and 2030 by country. The countries shown are the ones for which the model's R^2 is higher than 0.5, when having the country as test dataset, and the ones for which NDC targets are available and for which there were enough pixels to calculate R^2. (**b**) Map of African countries comparing the projected 2030 change with the declared NDC target. Countries in red are those where the model's R^2 falls below 0.5 when the country is used as the test dataset. Countries in grey lack available NDC data or do not have a sufficient number of pixels to calculate R^2.

Received: 4 July 2025; Accepted: 24 September 2026
Published online: 15 October 2026

References

1. Geiges, A. et al. Incremental improvements of 2030 targets insufficient to achieve the paris agreement goals. *Earth Syst. Dyn.* **11** (3), 697–708. https://doi.org/10.5194/esd-11-697-2020 (2020).
2. Roelfsema, M. et al. Taking stock of national climate policies to evaluate implementation of the paris agreement. *Nat. Commun.* **11** (1), 2096. https://doi.org/10.1038/s41467-020-15414-6 (2020).
3. Huggins, A. The Paris agreement's article 15 mechanism: An incomplete compliance strategy. In (eds Mayer, B. & Zahar, A.) 99–110 (Cambridge University Press, 2021).
4. Archer, D. & Brovkin, V. The millennial atmospheric lifetime of anthropogenic co_2. *Climatic Change* **90** (3), 283–297. https://doi.org/10.1007/s10584-008-9413-1 (2008).
5. Lan, X., Thoning, K. W. & Dlugokencky, E. J. Trends in globally-averaged CH_4, N_2O, and SF_6 determined from NOAA Global Monitoring Laboratory measurements. https://doi.org/10.15138/P8XG-AA10 (2025).
6. Jongaramrungruang, S., Matheou, G., Thorpe, A. K., Zeng, Z.-C. & Frankenberg, C. Remote sensing of methane plumes: instrument tradeoff analysis for detecting and quantifying local sources at global scale. *Atmos. Meas.Techn.* **14** (12), 7999–8017. https://doi.org/10.5194/amt-14-7999-2021 (2021).
7. Rijsdijk, P. et al. Quantifying uncertainties in satellite no2 superobservations for data assimilation and model evaluation. *Geosci. Model Dev.* **18** (2), 483–509. https://doi.org/10.5194/gmd-18-483-2025 (2025).
8. Lange, K., Richter, A. & Burrows, J. P. Variability of nitrogen oxide emission fluxes and lifetimes estimated from sentinel-5p tropomi observations. *Atmos. Chem. Phys.* **22** (4), 2745–2767. https://doi.org/10.5194/acp-22-2745-2022 (2022).
9. Munir, S., Mayfield, M., & Coca, D. Understanding spatial variability of no2 in urban areas using spatial modelling and data fusion approaches. *Atmosphere* **12** (2) https://doi.org/10.3390/atmos12020179 (2021).
10. Liu, F. et al. High-resolution mapping of nitrogen oxide emissions in large us cities from tropomi retrievals of tropospheric nitrogen dioxide columns. *Atmos. Chem. Phys.* **24** (6), 3717–3728. https://doi.org/10.5194/acp-24-3717-2024 (2024).
11. Kakooei, M., & Baleghi, Y. Spatial-temporal analysis of urban environmental variables using building height features. *Urban Climate* **52**, 101736 https://doi.org/10.1016/j.uclim.2023.101736 (2023).
12. Zhang, Z., Wang, J. & Lu, W. Exposure to nitrogen dioxide and chronic obstructive pulmonary disease (copd) in adults: a systematic review and meta-analysis. *Environ. Sci. Pollut. Res.* **25** (15), 15133–15145. https://doi.org/10.1007/s11356-018-1629-7 (2018).
13. Pettersson, M., Kakooei, M., Ortheden, J., Johansson, F. & Daoud, A. Time series of satellite imagery improve deep learning estimates of neighborhood-level poverty in africa 6165–6173. https://doi.org/10.24963/ijcai.2023/684 (2023).
14. Pettersson, M. B., Jerzak, C. T. & Daoud, A. Debiasing machine learning predictions for causal inference without additional ground truth data: one map, many trials in satellite-driven poverty analysis. In *Proceedings of the AAAI Conference on Artificial Intelligence* **40**, 39106–39115 (2026).
15. Li, H., Qiu, J. & Zheng, B. Air-pollution-satellite-based co_2 emission inversion: system evaluation, sensitivity analysis, and future research direction. *Atmos. Chem. Phys.* **25** (3), 1949–1963. https://doi.org/10.5194/acp-25-1949-2025 (2025).
16. Qu, Z. et al. Sector-based top-down estimates of nox, so2, and co emissions in east asia. *Geophys. Res. Lett.* **49** (2), 2021–096009. https://agupubs.onlinelibrary.wiley.com/doi/pdf/10.1029/2021GL096009 (2022).

17. Teorell, J., Sundström, A., Holmberg, S., Rothstein, B., Pachon, N.A., Phiri, V.S., Chen, C., & Liu, Z. The Quality of Government Standard Dataset, version Jan26. University of Gothenburg: The Quality of Government Institute. https://doi.org/10.18157/qogstdjan26 (2026).
18. Redi, T. Systematic review of air pollution in ethiopia: Focusing on indoor and outdoor sources, health, environment, economy impacts and regulatory frameworks. *F1000Research* **13**, 1385 https://doi.org/10.12688/f1000research.157621.1 (2024).
19. Adeniyi, O. & Folarin, O. Industrialization, finance, and urbanization in africa. *J. Afr. Dev.* **26** (1), 137–164. https://doi.org/10.5325/jafrideve.26.1.0137 (2025).
20. Air Pollution – East Africa (ASAP-East Africa), A.S.A. A systems approach to air pollution – east africa: Synthesis report. Technical report, UK Department for International Development. (accessed 07 February 2025); https://assets.publishing.service.gov.uk/media/5eb16ef186650c4356562f91/ASAP_-_Air_Pollution_in_East_Africa_-_Synthesis_Report.pdf (2020).
21. Qu, H., Suphachalasai, S., Thube, S., & Walker, S. South africa carbon pricing and climate mitigation policy. Selected Issues Paper SIP/2023/040, International Monetary Fund. (accessed 07 February 2025); https://www.imf.org/en/Publications/selected-issues-papers/Issues/2023/06/26/South-Africa-Carbon-Pricing-and-Climate-Mitigation-Policy-South-Africa-535220 (2023).
22. South Africa, G. South Africa's First Nationally Determined Contribution under the Paris Agreement: Updated September 2021. (accessed 07 February 2025); https://unfccc.int/sites/default/files/NDC/2022-06/South%74720Africa%20updated%20first%20NDC%20September%202021.pdf.
23. Ellerbeck, S. These start-ups are helping to make life in the sahel more sustainable. World Economic Forum. (accessed 07 February 2025); (2023).
24. Sun, W. et al. Long-term trends of anthropogenic so2, nox, co, and nmvocs emissions in china. *Earth's Fut.* **6** (8), 1112–1133. https://doi.org/10.1029/2018EF000822 (2018).
25. Scheibenreif, L., Mommert, M., & Borth, D. Estimation of air pollution with remote sensing data: Revealing greenhouse gas emissions from space. https://arxiv.org/abs/2108.13902 (2021).
26. Santos, T.C.D., Araujo, E.C., Silva, T.A.D., Freire, E.V., Landulfo, E., & Andrade, M.D.F. Emissions from fuel combustion by stoves in residential kitchens in são paulo – brazil. EGUsphere 2025, 1–18 https://doi.org/10.5194/egusphere-2025-968 (2025).
27. Smits, J. & Steendijk, R. The international wealth index (iwi). *Soc. Indicat. Res.* **122** (1), 65–85. https://doi.org/10.1007/s11205-014-0683-x (2015).
28. Crisp, D. et al. The on-orbit performance of the orbiting carbon observatory-2 (oco-2) instrument and its radiometrically calibrated products. *Atmos. Meas. Tech.* **10**(1), 59–81. https://doi.org/10.5194/amt-10-59-2017 (2017).
29. NASA/GSFC/GMAO Carbon Group: OCO-2 GEOS Level 3 monthly, 0.5x0.625 assimilated CO2 V10r (OCO2_GEOS_L3CO2_MONTH) at GES DISC. NASA Goddard Earth Sciences Data and Information Services Center (GES DISC). (accessed 23 April 2026); https://doi.org/10.5067/BGFIODET3HZ8 (2021).
30. Bichler, R., & Bittner, M. Comparison between economic growth and satellite-based measurements of no2 pollution over northern italy. *Atmos. Environ.* **272**, 118948 https://doi.org/10.1016/j.atmosenv.2022.118948 (2022).
31. European Space Agency: Sentinel-5P Nitrogen Dioxide Level 2 Product Readme File. Issue 2.4; (accessed 2026); https://sentinel.esa.int/documents/247904/3541451/Sentinel-5P-Nitrogen-Dioxide-Level-2-Product-Readme-File (2023).
32. Geffen, J. et al. Sentinel-5p tropomi no_2 retrieval: impact of version v2.2 improvements and comparisons with omi and ground-based data. *Atmos. Meas. Tech.* **15** (7), 2037–2060. https://doi.org/10.5194/amt-15-2037-2022 (2022).
33. Judd, L. M. et al. Evaluating sentinel-5p tropomi tropospheric no_2 column densities with airborne and pandora spectrometers near new york city and long island sound. *Atmos. Meas. Tech.* **13** (11), 6113–6140. https://doi.org/10.5194/amt-13-6113-2020 (2020).
34. Geddes, J. A., Martin, R. V., Bucsela, E. J., McLinden, C. A. & Cunningham, D. J. M. Stratosphere-troposphere separation of nitrogen dioxide columns from the tempo geostationary satellite instrument. *Atmos. Meas. Tech.* **11** (11), 6271–6287. https://doi.org/10.5194/amt-11-6271-2018 (2018).
35. United Nations Framework Convention on Climate Change: Nationally Determined Contributions (NDCs). (accessed 25 September 2026); https://unfccc.int/process-and-meetings/the-paris-agreement/nationally-determined-contributions-ndcs
36. United Nations Framework Convention on Climate Change: Nationally Determined Contributions (NDCs) Registry. (accessed 25 September 2026); https://unfccc.int/NDCREG
37. Fuentes Andrade, B. et al. A method for estimating localized co_2 emissions from co-located satellite xco_2 and no_2 images. *Atmos. Meas. Tech.* **17** (3), 1145–1173. https://doi.org/10.5194/amt-17-1145-2024 (2024).
38. Pettersson, M.B. Temporal neighborhood-level material wealth maps of Africa (1990-2019). Harvard Dataverse. (accessed 25 September 2026); https://doi.org/10.7910/DVN/9DINV4 (2023).
39. Copernicus Sentinel-5P (processed by ESA): TROPOMI level 2 nitrogen dioxide total column products, Version 02. European Space Agency. (accessed 25 September 2026); https://doi.org/10.5270/S5P-9bnp8q8 (2021).

Author contributions

FG: Preprocessed NO2 and IWI data. Developed and trained the models. Made calculations and plots. Wrote most of the text. Contributed to interpretation of results. Proofread the text. Discussions. MK: Contributed to interpretation of results. Proofread the text. Discussions. AD: Contributed to interpretation of results. Proofread the text. Discussions.

Funding

This work was supported by the Swedish Research Council (Vetenskapsrådet) under grant number 2023-06608.

Declarations

Competing interests

The authors declare no competing interests.

Additional information

Correspondence and requests for materials should be addressed to F.G.

Reprints and permissions information is available at www.nature.com/reprints.

Publisher's note Springer Nature remains neutral with regard to jurisdictional claims in published maps and institutional affiliations.

Open Access This article is licensed under a Creative Commons Attribution 4.0 International License, which permits use, sharing, adaptation, distribution and reproduction in any medium or format, as long as you give appropriate credit to the original author(s) and the source, provide a link to the Creative Commons licence, and indicate if changes were made. The images or other third party material in this article are included in the article's Creative Commons licence, unless indicated otherwise in a credit line to the material. If material is not included in the article's Creative Commons licence and your intended use is not permitted by statutory regulation or exceeds the permitted use, you will need to obtain permission directly from the copyright holder. To view a copy of this licence, visit http://creativecommons.org/licenses/by/4.0/.

© The Author(s) 2026